Reaction Kinetics, Mechanisms and Catalysis (2022) 135:847–865
https://doi.org/10.1007/s11144-022-02179-w

Experimental and kinetic study of vacuum residue cracking over zirconium based catalysts

Aya Abd Al-Karim[1] · Zaidoon M. Shakor[1] · Farooq Al-Sheikh[1] · William A. Anderson[2]

Received: 7 December 2021 / Accepted: 30 January 2022 / Published online: 7 February 2022

Abstract

In this study, thermal cracking and catalytic cracking over zirconium-based catalysts of the vacuum residue were achieved in the presence of supercritical steam at 400–450 °C, 20 bar, and 2–4 h. Two different catalysts (ZrFeNi and ZrCoNi) were prepared using a sol–gel precipitation method and characterized using X-ray diffraction, EDX-spectrum, scanning electron microscopy, and BET surface area. The results showed the lowest VR conversion was achieved in the thermal cracking, catalytic cracking using ZrFeNi and catalytic cracking using ZrCoNi were 31.7, 35.3, and 38% while the highest VR conversion was achieved in the thermal cracking, catalytic cracking using ZrFeNi and catalytic cracking using ZrCoNi were 38.6, 71.1 and 76.3%. A new kinetic model of the eight lumps and 28 reaction steps were developed to describe the VR cracking while a genetic algorithm optimization method was used to predict the optimum set of kinetic parameters in which all computations were achieved using MATLAB version 2020a.

Keywords Vacuum residue · Zirconia catalyst · Catalytic cracking · Kinetic model · Aspen Hysys

Abbreviations

XRD	X-ray powder diffraction
SEM	Scanning electron microscopy
BET	Brunauer, Emmett, and Teller
ASTM	Atmospheric standard test method
APD	Average pore diameter
PID	Proportinal integral derivative
CSTR	Continuous stirred tank reactor

✉ Farooq Al-Sheikh
faalshei@uwaterloo.ca; Farooq.a.mehdi@uotechnology.edu.iq

[1] Chemical Engineering Department, University of Technology, Baghdad, Iraq

[2] Chemical Engineering Department, University of Waterloo, Waterloo, ON, Canada

RHC	Residue hydrocracking
MAE	Mean absolute error
MRE	Mean relative error
GA	Genetic algorithms
AR	Atmospheric residue
VR	Vacuum residue
LN	Light naphtha
HN	Heavy naphtha
Ke	Kerosene
LGO	Light gas oil
HGO	Heavy gas oil
LVGO	Light vacuum gas oil
HVGO	Heavy vacuum gas oil

Introduction

Petroleum refining industries have faced several challenges in the past few years. One of those challenges is an increase in demand for the light fractions and a decreasing ratio of the exploited light crude oils since crude oil refining yields 10–15% vacuum residue (VR) depending on the crude oil origin. Thermal and catalytic cracking is usually used to upgrade the vacuum residue (VR) and increase the distillation profit. In cracking, the heavier long-chain hydrocarbons are broken down into lighter ones by breaking carbon–carbon bonds while the cracking rate and final products strongly depend on the temperature, pressure, and presence of catalysts [1]. Fumoto et al. performed catalytic cracking of Canadian oil sand bitumen using zirconia-alumina-iron oxide catalyst at 450–500 °C in the presence of steam. The largest yield of light oil at 500 °C temperature and 2 h residence time was approximately 50 mol% with no coke formation [2]. Gai et al. studied the use of sub- and supercritical water to provide a unique homogenous acidic-reaction system of bitumen cracking in an H_2 or N_2 atmosphere using an activated carbon-supported nickel catalyst [3]. Ahn et al. performed vacuum residue upgrading using subcritical water and a catalyst and compared the liquid product conversion. The maximum conversion of 55.5 wt% was given at 400 °C, 0.5 g catalyst, 6 h reaction time, and 20 g of water, and it was found that an accumulation of a mass of 61.2 wt% at 500 °C of the liquid product was accomplished by conversion of the light product with a low boiling point [4]. Do et al. used a NiK/CeO_2 catalyst to investigate the interaction between a Ni metal, and CeO_2 support and its effect on the oxidative cracking of VR. The addition of NiK provided Ni metallic of hydrogenation and produced a lot of liquid products like diesel which was the highest one with 22.87 wt% without a catalyst [5]. Nguyen-Huy et al. prepared and tested NiK/CeZr-Al catalysts cracking of the vacuum residue with steam using a fixed-bed reactor at 500 °C and 1 atm [6]. Yunanto et al. used active alumina oxide (Al_2O_3) in a pyrolysis process with a single-stage under thermal and catalytic cracking of the VR. The process was carried out at 450 °C and varied reaction times (5–30 min) in the fixed-batch reactor. They found that in the thermal process, the liquid was produced with the highest saturates

content, while in the catalytic process liquid was produced with the highest aromatics and olefins contents [7]. Puron et al. prepaid support for hydrocracking catalysts using Ni, and Mo, impregnated Cr-doped alumina ($NiMo/Al_2O_3$), tested catalytic activity in HDA, HDS, and HDM of the Maya VR in a batch reactor at 425 °C and compared with NiMo supported. They found that the Cr aided metal dispersion in the catalyst synthesis and coke dispersion during the reaction. The spent catalyst showed reductions in the surface area and pore volume while a $NiMo/ Al_2O_3$ catalyst had a decrease in the average pore diameter (APD) [8]. The previous work concerned with vacuum residue cracking is summarized in Table 1.

In this research, we expand on these studies by manufacturing, characterizing, and using two zirconium-based catalysts in steam catalytic cracking of the vacuum residue cracking and developing a new kinetic model to describe this catalytic cracking over ZrFeNi catalyst. Experimental data were obtained from runs carried out in a batch reactor at three different temperatures (400, 425, and 450 °C), reaction times (2, 3, and 4 h), and catalyst weights (0.5, 1, and 1.5 g).

Materials and methods

A real vacuum residue from a vacuum distillation unit was supplied by the domestic Al-Doura petroleum refinery, Baghdad, Iraq while all chemicals [iron oxide (Fe_2O_3, 98%), zirconium nitrate ($Zr(NO_3)_4$, 99%), nickel nitrate ($Ni(NO_3)_2$, 98.5%), cobalt nitrate ($Ni(NO_3)_2$, 98%), and distilled water (H_2O, 100%)] were purchased from local suppliers. Table S1 shows the properties of the vacuum residue while Table S2 shows distillation data of the feed. Two different catalysts were manufactured: The first one was composed of a mixture of nickel nitrate and zirconium nitrate with iron oxide, while the second was composed of a mixture of zirconium nitrate, nickel nitrate, and cobalt nitrate. The mixture was dissolved in distilled water and heated for 1 h at 60 °C. After heating, ammonia solution was added to the solution to adjust the pH to 10 with continuous heating for 30 min. Slurries were evaporated using a rotary evaporator while the solid phase appeared in the bottom of the evaporation vessel. The mixture was then cooled to separate the solid phase using a filter paper, dried at 25 ± 1 °C for 24 h, and finally calcined at 600 °C for 4 h. The crystalline construction of the two catalysts was analyzed by X-ray diffraction (LabX XRD-6000, Shimadzu Corporation) at 25 ± 1 °C using a powder diffractometer between 10° and 90° in a step of 0.02 with the Cu Kα radiation. The morphological structure of the synthesized catalyst samples was obtained using scanning electron microscopy. The surface area and pore size of the catalysts were estimated using a surface area analyzer (Vega3 Tescan) by N_2 adsorption/desorption at 25 °C which is also known as Brunauer–Emmett–Teller (BET) method. The cracking was performed in a 200 ml stainless steel batch autoclave equipped with a 2000-W heater and a PID controller to control the temperature. Required amounts of the vacuum residue, water, and catalyst were placed into the autoclave reactor and then closed well using eight stainless-steel 304 bolts. The temperature was linearly adjusted to increase from 25 ± 1 °C to the desired one using a PID controller. The time required to reach the reaction temperature was within the range of 105–132 min depending on the desired reaction

Table 1 A summary of the previous work concerning VR cracking

Catalyst	Reactor type	Fuel type	Temperature (°C)	Pressure	Surface area (m^2/g)	Volume (m^3/g)	References
N/A	Batch	VR	400–530	atm-12 kg/cm^2	N/A	400 ml	[9]
MoS_2	Semi-batch	Cold lake VR	415	5.5 Mpa	N/A	N/A	[10]
N/A	Batch	Petroleum residual oil	400–480	120–180 kpa	N/A	N/A	[11]
N/A	Semi-batch	Kuwait VR	400–430	N/A	N/A	N/A	[12]
Ni-MO/Al_2O_3	Ebullated bed	VR	401–412	18–20 mpa	N/A	N/A	[13]
Iron oxide containing zirconia and alumina	Fixed bed	AR	475	atm	N/A	N/A	[14]
ZrO_2	Batch	VR	470	N/A	High	N/A	[15]
O_2 and raw material	Continuous flow	Heavy oil residue	430–460	2–8 atm	N/A	N/A	[16]
Ni/k	N/A	DeasphaLted VR	435–445	300 psig	N/A	N/A	[17]
CeZr, FeCoCeZr1, FeCoCeZr2	Fixed bed	Oil sand bitumen	470	N/A	N/A	N/A	[18]
N/A	Batch	AR andVR	400	N/A	N/A	100 ml	[19]
Calcium aluminate, FCC catalyst, and ZSM-5 zeolites	Fixed bed dual	VR	600–750	N/A	N/A	N/A	[20]
Fe–Mn mixed metal oxide	Fixed bed	VR	550	atm	N/A	N/A	[21]
Calcium aluminate and FCC catalyst	Fluidized bed and fixed bed	VR	300	N/A	342	0.17	[22]
Presulfied oil-soluble MoS_2	Batch	VR	410	10 MPa	N/A	N/A	[23]

temperature. The reaction time started when the reaction temperature was achieved for the first time by the controller while the reactor pressure increased directly with the reaction temperature, increasing slightly during the reaction duration. At the end of the reaction duration, the heater was turned off and the reactor was left to cool again to 25 ± 1 °C. Then, water was separated from the reaction mixture by gravity while the catalyst was separated using a mesh. Vacuum distillation (VDS3000, Kohlar company) was used to fractionate the cracking products depending on the boiling point range and to determine the range of the petroleum products boiling points that could be completely or partially vaporized at 450 °C (maximum liquid temperature). The sample was distilled at a controlled reduced pressure of 10 mmHg under conditions that were designed to provide approximately one notional plate fractionation. Initial and final boiling points were measured to find the distillation curve relating the volume percent distilled and atmospheric equivalent boiling point temperatures. Then, the produced distillation curves ASTM D1160 (Vacuum distillation) were converted to ASTM D86 (atmospheric distillation) using Aspen Hysys software. Therefore, the light cuts were calculated using a typical crude oil cut point presents in Table 2. Also, curves of the true boiling point (TBP) of 15 experiments are presented in Figs. S1–15 in the supplementary material.

Kinetic model

The kinetic modeling describes dynamic composition changes of the cracking products with a subsequent formation of gas and coke as a result of the catalytic cracking [24–26]. Singh et al. developed a five-lumps kinetic model using ten reactions of vacuum residue thermal cracking where two residue feedstocks were of Indian and Mithe middle East origin estimated from Indian refineries. The reaction pathways included gasoline, LPG, gas, and vacuum gas oil lumps [9]. Martinez and Ancheyta investigated a five-lump kinetic model of heavy oil hydrocracking in a CSTR reactor over a temperature range 380–420 °C and found that the lighter lumps are more sensitive to the temperature change, while heavier lumps are hydrocracked more easily and the mean absolute error of the developed kinetic model was less than 5% [27].

Table 2 Typical crude oil cut points (ASTM D86)

Cut	IBP (°C)	EP (°C)
Off gas	–	32
Light naphtha	32	88
Heavy naphtha	88	193
Kerosene	193	271
Light gas oil	271	321
Heavy gas oil	321	425
Light vacuum gas oil	425	510
Heavy vacuum gas oil	510	564
Vacuum residue	565	–

Gao et al. developed an eight-lumps kinetic model that had 20 reactions and one catalyst deactivation term for vacuum residue catalytic cracking, which were CP, CN, CA, HCO, LPG, dry gas, light oil, and coke. The experimental data were obtained using a fixed bed reactor in a pilot plant at four different temperatures 460, 480, 500, and 520 °C and their model demonstrated high simulation accuracy with the predicted yields being in close agreement with the experimental results [28]. Manek and Haydary developed a kinetic model of tR hydrocracking based on the datasets estimated from a commercial residue hydrocracking unit (RHC). The temperature and pressure were in the range 401–412 °C and 18–20 MPa, while the kinetic model included six fractions (gas, naphtha, kerosene, gas oil, vacuum distillate, and vacuum residue) and eight reaction steps [13]. Cabrales-Navarro and Pereira-Almao used a Ni/K catalyst in catalytic steam cracking of the VR at 435–445 °C and 300 psig. Their lumped kinetic model was evaluated including asphaltenes generation while heavy vacuum gas oil (HVGO) and light vacuum gas oil (LGVO) fractions were determined to be much more reactive under the catalytic steam cracking operating condition [17]. Kaminski and Husein used three different schemes of the five-lump model based on gas, coke, asphaltene, maltene, and distillate fraction in thermal cracking of VR and AR. The process was carried out in a batch reactor at 400–420 °C and 3–5 kPa while the kinetic parameters were estimated from the benchmarking between experimental and predicted results. They found that the composition difference between atmospheric residue (AR) and vacuum residue (VR) in terms of asphaltene, and hydrogen donor nature and the content most likely led to rapid catalyst deactivation and a loss of the selective cracking mechanism experienced during AR cracking [19]. Table 3 shows a summary of the previous work concerned with kinetic modeling of VR cracking. In this study, the first-order developed simplified kinetic model [9, 12, 17, 19, 31] is presented in Fig. 1 while Table 4 was used containing eight lumps [light naphtha (LN), heavy naphtha (HN), light gas oil (LGN), heavy gas oil (HGO), light vacuum gas oil (LVGO), heavy vacuum gas oil (HVGO), and vacuum residue (VR)] and 28 reactions using some reasonable assumptions [18]: (1) Uniform concentration and temperature, (2) Power-law kinetic model and (3) Neglecting the pressure effects and gaseous products due to the smaller weights compared to other liquids products. The reaction rate equations of each lump represented in Eqs. 1–8:

$$\frac{d[LN]}{dt} = K_{22}[VR] + K_{16}[HVGO] + K_{11}[LVGO] + K_{7}[HGO] + K_{4}[LGO] + K_{2}[Ke] + K_{1}[HN] \tag{1}$$

$$\frac{d[HN]}{dt} = K_{23}[VR] + K_{17}[HVGO] + K_{12}[LVGO] + K_{8}[HGO] + K_{5}[LGO] + K_{3}[Ke] - K_{1}[HN] \tag{2}$$

$$\frac{d[Ke]}{dt} = K_{24}[VR] + K_{18}[HVGO] + K_{13}[LVGO] + K_{9}[HGO] + K_{6}[LGO] - K_{2}[Ke] - K_{3}[Ke] \tag{3}$$

$$\frac{d[LGO]}{dt} = K_{25}[VR] + K_{19}[HVGO] + K_{14}[LVGO] + K_{10}[HGO] - K_{4}[LGO] - K_{5}[LGO] - K_{6}[LGO] \tag{4}$$

Table 3 A summary of the previous work concerning kinetic modeling of VR cracking

Catalyst	Fuel type	Reactor type	Temperature (°C)	Pressure	No. lump	References
$NaNO_3$, KNO_3 and $NaNO_2$	VR	Batch	400–530	atm-12 kg/cm^2	Five	[9]
NiO/Ni and MoO_3/Mo	Heavy oil	CSTBR	380–420	100 kg/cm^2	Five	[27]
Without catalyst	Kuwaiti VR	Semi batch	400–430	atm	Five	[12]
Commercial equilibrium catalyst LVR	VR	Fixed fluidized bed	460–520	N/A	Eight	[28]
Ni-Mo/Al_2O_3	VR	CSTR	401–412	18–20 MPa	Six	[13]
Ammonium phosphomolybdate	Heavy residue	Batch	405–435	7.0 MPa	Six	[29]
Without catalyst	Vacuum pyrolysis of POA	Semi batch	410–450	40 kPa	Five	[30]
Without catalyst	VR	Batch	400–430	12 kg/cm^2	Six	[31]
Ni/K	Deasphalted VR	Batch	435–445	300 psig	Eight	[17]
Without catalyst	AR and VR	Batch	400–420	3–5 kpa	Five	[19]

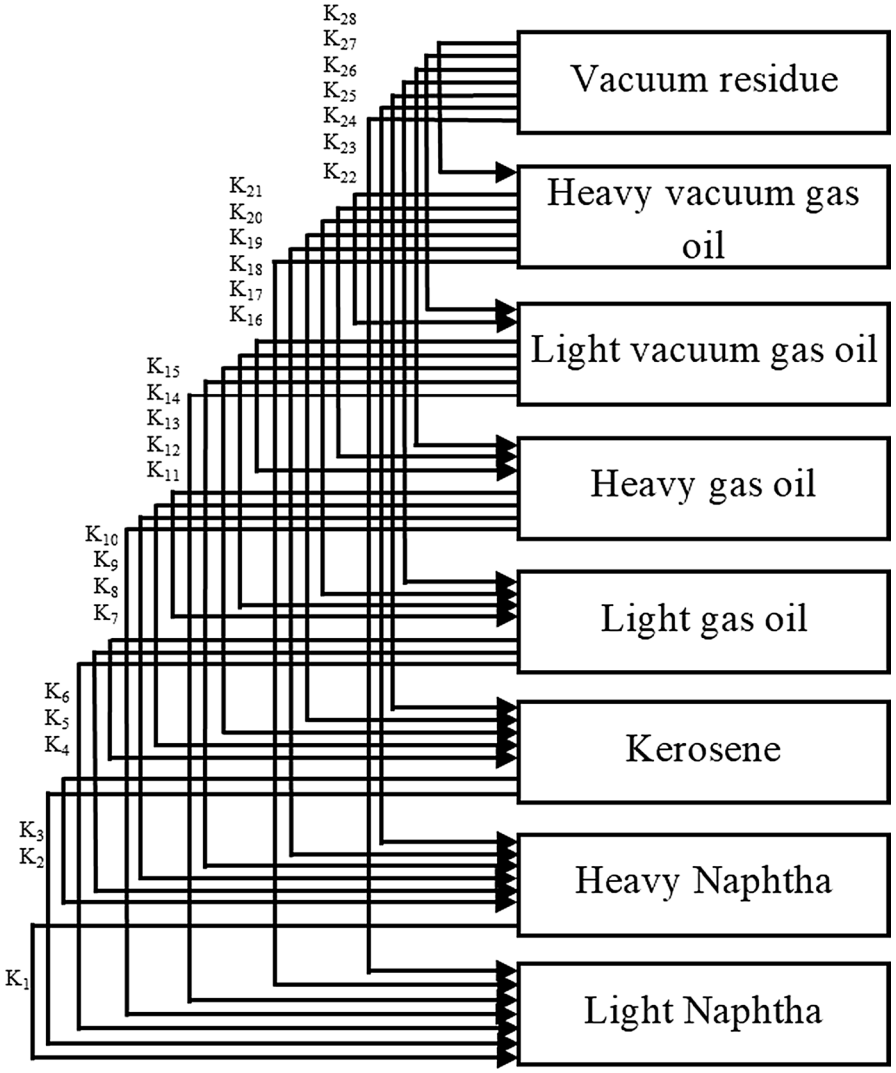

Fig. 1 Eight-lump kinetic model of the VR cracking

$$\frac{d[HGO]}{dt} = K_{26}[VR] + K_{20}[HVGO] + K_{15}[LVGO] - K_7[HGO] - K_8[HGO] - K_9[HGO] - K_{10}[HGO] \quad (5)$$

$$\frac{d[LVGO]}{dt} = K_{27}[VR] + K_{21}[HVGO] - K_{11}[LVGO] - K_{12}[LVGO] - K_{13}[LVGO] - K_{14}[LVGO] - K_{15}[LVGO] \quad (6)$$

$$\frac{d[HVGO]}{dt} = K_{28}[VR] - K_{16}[HVGO] - K_{17}[HVGO] - K_{18}[HVGO] - K_{19}[HVGO] - K_{20}[HVGO] - K_{21}[HVGO] \quad (7)$$

Table 4 Predicted kinetic parameters

Reaction	Kinetic parameter	Rate constant	
		Ao	E (J/mol K)
Heavy naphtha → Light naphtha	K_1	5.65×10^{4}	271,795
Kerosene → Light naphtha	K_2	3.23×10^{5}	263,815
Kerosene → Heavy naphtha	K_3	3.92×10^{8}	151,625
Light gas oil → Light naphtha	K_4	8.95×10^{4}	289,917
Light gas oil → Heavy naphtha	K_5	1.05×10^{8}	298,014
Light gas oil → Kerosene	K_6	3.84	45,121
Heavy gas oil → Light naphtha	K_7	4.23×10^{6}	282,718
Heavy gas oil → Heavy naphtha	K_8	5.95×10^{7}	290,029
Heavy gas oil → Kerosene	K_9	1.23×10^{4}	298,313
Heavy gas oil → Light gas oil	K_{10}	3.73×10^{7}	159,535
Lightvaccum gas oil → Light naphtha	K_{11}	1.98×10^{4}	286,901
Light vacuum gas oil → Heavy naphtha	K_{12}	1.48	39,517
Light vacuum gas oil → Kerosene	K_{13}	1.66×10^{7}	289,828
Light vacuum gas oil → Light gas oil	K_{14}	4.79×10^{6}	155,871
Light vacuum gas oil → Heavy gas oil	K_{15}	3.64	35,645
Heavy vacuum gas oil → Light naphtha	K_{16}	319	267,809
Heavy vacuum gas oil → Heavy naphtha	K_{17}	7.02×10^{6}	297,038
Heavy vacuum gas oil → Kerosene	K_{18}	1.02×10^{6}	274,023
Heavy vacuum gas oil → Light gas oil	K_{19}	3.06×10^{5}	130,896
Heavy vacuum gas oil → Heavy gas oil	K_{20}	4.65×10^{15}	251,554
Heavy vacuum gas oil → Light vacuum gas oil	K_{21}	1.91×10^{17}	283,187
Vacuum residue → Light naphtha	K_{22}	4.06×10^{-3}	24,032
Vacuum residue → Heavy naphtha	K_{23}	2.21×10^{4}	110,863
Vacuum residue → Kerosene	K_{24}	1.89×10^{-2}	22,901
Vacuum residue → Light gas oil	K_{25}	1.58E	49,339
Vacuum residue → Heavy gas oil	K_{26}	13.3	63,904
Vacuum residue → Light vacuum gas oil	K_{27}	0.238	27,420
Vacuum residue → Heavy vacuum gas oil	K_{28}	5.99×10^{4}	103,075

$$\frac{d[VR]}{dt} = -K_{22}[VR] - K_{23}[VR] - K_{24}[VR] - K_{25}[VR] - K_{26}[VR] - K_{27}[VR] - K_{28}[VR] \tag{8}$$

$$K = A_o e^{-E/RT} \tag{9}$$

Here A_o is the pre-exponential factor, E is activation energy (J/mol), R is the universal gas constant (8.314 J/mol K) and T is the absolute temperature (K). The mean relative error (MAE) and mean absolute error (MRE) were used to evaluate a sensitivity analysis on the developed kinetic model using Eqs. 10 and 11 [13, 28]:

$$\mathrm{MAE} = \frac{1}{\mathrm{N} \times \mathrm{M}} \sum_{\mathrm{j}=1}^{\mathrm{M}} \sum_{\mathrm{i}=1}^{\mathrm{N}} \left| \mathrm{y}_{\mathrm{i,j}}^{\mathrm{exp}} - \mathrm{y}_{\mathrm{i,j}}^{\mathrm{pred}} \right| \tag{10}$$

$$\mathrm{MRE} = \frac{1}{\mathrm{N} \times \mathrm{M}} \sum_{\mathrm{j}=1}^{\mathrm{M}} \sum_{\mathrm{i}=1}^{\mathrm{N}} \left(\frac{\mathrm{y}_{\mathrm{i,j}}^{\mathrm{exp}} - \mathrm{y}_{\mathrm{i,j}}^{\mathrm{pred}}}{\mathrm{y}_{\mathrm{i,j}}^{\mathrm{exp}}} \right) \tag{11}$$

Here N, M, $\mathrm{y}_{\mathrm{i,j}}^{\mathrm{exp}}$, and $\mathrm{y}_{\mathrm{i,j}}^{\mathrm{pred}}$ are the components number, dataset number, experimental weight fraction values, and predicted weight fraction values. The percentage VR conversion and percentage yield in the weight fraction for cracking products were calculated using Eqs. 12 and 13.

$$\%\ \text{VR conversion (Wt)} = \left(\frac{\text{Weight VR feed} - \text{Weight VR Out}}{\text{Weight VR feed}} \right) \times 100 \tag{12}$$

$$\%\ \text{Desired product yield (Wt)} = \left(\frac{\text{Weight of desired product}}{\text{Weight VR feed}} \right) \times 100 \tag{13}$$

Average molecular weights were used to convert the reactant and products weights to moles and vice and were calculated as follows [28, 32]:

$$\overline{MW} = \frac{\sum_{i=1}^{n} C_i MW_i}{\sum_{i=1}^{n} C_i} \tag{14}$$

Here MW is the average molecular weight of the lump, g/mol and Ci is the concentration of the lump i, mol/g. The reaction stoichiometry for a specific reaction was calculated by dividing the average molecular weights of reactants by the average molecular weight of the products.

$$v_{ij} = \frac{MW_i}{MW_j} \tag{15}$$

Here v_{ij} the stoichiometric coefficient. A genetic algorithm optimization method was used to predict an optimum set of the kinetic parameters where all computations were achieved using MATLAB version 2020a.

Results and discussion

Catalyst characterization

The crystalline construction of the two catalysts was analyzed by X-ray diffraction at 25 ± 1 °C using a powder diffractometer between 10° and 90° in a step of 0.02 with the Cu K_α radiation. Fig. 2A and B show the X-ray diffraction (XRD)

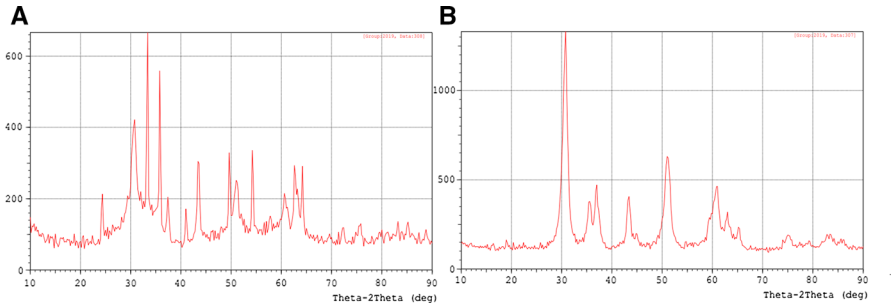

Fig. 2 **A** XRD-pattern of ZrFeNi catalyst. **B** XRD-pattern of ZrCoNi catalyst

patterns of both calcined ZrFeNi and ZrCoNi powder, where the peaks observed at $2\theta = 30.7°$, 35.8°, 50.9°, 60.2°, and 62.8° are the metastable tetragonal ZrO_2 while the peak observed at $2\theta = 28.2°$ is monoclinic zirconia. For the calcined catalyst, peaks at $2\theta = 37.4°$ and 43.4°, corresponding to Ni can be observed. These can be assigned to (111) and (200) of the lattice plane of the cubic Ni. For the reduced sample, Ni disappears completely and two small peaks corresponding to metallic nickel at $2\theta = 44.6°$ and 51.8°. A morphological structure of the synthetic catalysts samples was obtained by utilizing scanning electron microscopy. A scanning electron microscopy (SEM) image of the two synthetic catalysts can be seen in Fig. 3A and B in which one of the catalyst crystals had a flat shape and a wavy edge while the other was a round shape and a wavy edge. Fig. 1A and B of the ZrFeNi and ZrCoNi catalysts in the Supplementary Material show the appearance of the other elements (O, Al, C, and S) in different percentages with catalysts while the active metals distribution was very well for both catalysts. The zirconium concentration in the ZrCoNi catalyst (29.2 wt%) was higher than that in the ZrFeNi catalyst (19.7 wt%). A range of the surface area of the typical catalyst was from 15 to 40 m^2/g. Increasing the number of the base active sites leads to an increase in the surface area of the catalyst. The ZrFeNi catalyst had a larger surface area than that of the ZrCoNi one

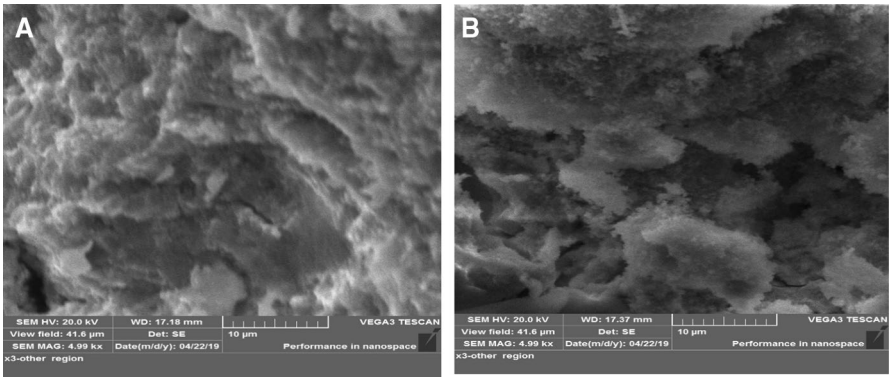

Fig. 3 **A** SEM image of ZrFeNi catalyst. **B** SEM image of ZrCoNi catalyst

because the Zr concentration in the ZrCoNi catalyst (29.2%) was higher than that in the ZrFeNi one (19.7%). Also, ZrO metal oxide has a smaller surface area (25 m^2/g) than other metal oxides. The BET surface area of the ZrFeNi and ZrCoNi catalysts were 47.1 and 26.0 m^2/g, respectively.

Analysis of thermal cracking

Results of the 15 experiments are summarized in Tables 5 and 6 which present the yield of all lumps and operating conditions applied in each experiment. Results of the thermal cracking at the reaction temperatures 400–425 °C with the same operating conditions were presented in Experiments 1 and 2 showing that the VR is mainly converted to HGO, LVGO, and HVGO and indicating that no strong VR cracking occurred without a catalyst. Also, long-chain hydrocarbons were cracked easier than short-chain ones while increasing the cracking temperature from 400 to 425 °C increased VR conversion from 25.8 to 28.2%.

Effect of operating variables on cracking yield

Catalyst weight effect

Experiments 3, 4, and 5 present a cracking yield using different catalyst amounts (0.5, 1, and 1.5 g) with the same operating conditions (ZrFeNi catalyst, 10 wt steam%, 400 °C reaction temperature, and 2 h reaction time). Using a catalyst in cracking produces different amounts of lighter fractions which denotes that using a catalyst decreases the activation energy of the cracking reactions. Increasing the catalyst weight from 0.5 to 1 g increases the VR conversion from 30.3 to 32.6%. The further increase in the catalyst weight to 1.5 g increases VR conversion to 37.9%. Also by comparing Experiments 1 and 3, the presence of the catalyst is seen to have a significant effect on the VR conversion increase.

Reaction temperature effect

Experiments 5, 6, and 7 present the cracking yield at different reaction temperatures (400, 425, and 450 °C) with the same operating conditions (ZrFeNi catalyst, 10 wt steam%, 1.5 g catalyst weight, and 2 h reaction time). Increasing the reaction temperature from 400 to 425 °C increased the VR conversion from 37.9 to 46.3%, and increasing the reaction temperature to 450 °C increased VR conversion to 51.4%. Higher reaction temperatures accounted for the higher VR and asphaltene conversions at the expense of the small increase in light and heavy naphtha yields.

Reaction time effect

Experiments 5, 8, and 9 present the cracking yield of different reaction times (2, 3, and 4 h) with the same operating conditions (ZrFeNi catalyst, 10 wt steam%, 400 °C, and 1.5 g catalyst weight). Increasing the reaction time from 2–3 h increased the

Table 5 Cracking products yield

No. of experiment	Light naphtha	Heavy naphtha	Kerosene	Light gas oil	Heavy gas oil	Light vacuum gas oil	Heavy vacuum gas oil	Vacuum residue
1	0.0062	0.0248	0.024	0.018	0.096	0.098	0.049	0.683
2	0.0054	0.0216	0.044	0.051	0.106	0.095	0.063	0.614
3	0.0014	0.0056	0.025	0.025	0.107	0.113	0.077	0.647
4	0.0082	0.0328	0.050	0.049	0.107	0.080	0.059	0.615
5	0.0104	0.0416	0.044	0.026	0.095	0.098	0.072	0.613
6	0.0120	0.0480	0.037	0.031	0.178	0.151	0.116	0.427
7	0.0066	0.0264	0.031	0.042	0.231	0.215	0.158	0.289
8	0.0014	0.0568	0.072	0.056	0.116	0.113	0.091	0.480
9	0.0076	0.0304	0.068	0.076	0.221	0.228	0.132	0.237
10	0.0076	0.0304	0.048	0.053	0.119	0.106	0.071	0.565
11	0.0088	0.0352	0.058	0.024	0.141	0.125	0.081	0.528
12	0.0076	0.0304	0.056	0.039	0.151	0.176	0.122	0.417
13	0.0066	0.0264	0.042	0.049	0.118	0.076	0.062	0.620
14	0.0136	0.0544	0.051	0.054	0.122	0.110	0.081	0.514
15	0.0140	0.0560	0.038	0.031	0.173	0.171	0.118	0.397

Table 6 Operating conditions of the experiments

No. of experiment	Temperature (°C)	Water Vol%	Catalyst weight (gm)	Time (h)	VR Source
1	400	10	0	2	Basra
2	425	10	0	2	Basra
3	400	10	0.5 FeNiZr	2	Basra
4	400	10	1 FeNiZr	2	Basra
5	400	10	1.5 FeNiZr	2	Basra
6	425	10	1.5 FeNiZr	2	Basra
7	450	10	1.5 FeNiZr	2	Basra
8	400	10	1.5 FeNiZr	3	Basra
9	400	10	1.5 FeNiZr	4	Basra
10	400	15	1.5 FeNiZr	2	Basra
11	400	20	1.5 FeNiZr	2	Basra
12	400	10	1.5 FeNiZr	2	Baghdad
13	400	10	1.5 CoNiZr	2	Basra
14	425	10	1.5 CoNiZr	2	Basra
15	450	10	1.5 CoNiZr	2	Basra

VR conversion from 37.9 to 41.6%, and further increasing the reaction time to 4 h increased VR conversion to 45.8%.

Steam percentage effect

Experiments 5, 10, and 11 present the cracking yield of different steam loading (10, 15, and 20 wt%) with the same operating conditions (ZrFeNi catalyst, 400 °C, 1.5 g catalyst weight, and 2 h reaction time). Increasing the steam loading from 10 to 15 wt% decreased the VR conversion from 37.9 to 32.9% and further increasing the steam loading to 20 wt% increased VR conversion to 35.2%. It can be recognized that there was an unexpected effect of steam percentage on VR, therefore the 10% steam was taken as the optimum steam ratio.

VR feed type effect

The catalytic cracking yield for two feedstock was compared with the same operating conditions (ZrFeNi catalyst, 400 °C, 1.5 g catalyst weight, and 2 h reaction time). Experiment 12 represents the cracking yield of the VR from the refinery located in East Baghdad, Iraq. As compared with Experiment 5, it can be recognized that the yield of lighter fractions was much greater than that in the case of using the Basra crude oil from the refinery located in Basra, Iraq instead of VR produced from vacuum distillation of light crude oil in East Baghdad, Iraq. This result is due to the lighter fractions of the Basra crude oil being greater than those of the VR of the East Baghdad heavy crude oil.

Catalyst type effect

Experiments 13, 14, and 15 present the cracking yield at different reaction temperatures (400, 425, and 450 °C) with the same operating conditions (ZrCoNi catalyst, 10 wt steam%, 1.5 g catalyst weight, and 2 h reaction time). Increasing the reaction temperature from 400 to 425 °C increased the VR conversion from 28.6 to 36.3% and further increasing the reaction temperature to 450 °C increased VR conversion to 40.6%. By comparing the cracking yield for the ZrCoNi catalyst with the cracking yield of the ZrFeNi catalyst, illustrated in Experiment 5, 6, and 7, it can be recognized that both catalysts are effective for catalytic cracking but the ZrFeNi catalyst is stronger than ZrCoNi one under the steam catalytic cracking operations used here.

Optimum operating conditions

The VR conversion and lighter products yield of the fifteen experiments are summarized in Figs. 4 and 5. It can be recognized that the lowest VR conversion (25.8 wt%) was achieved at 400 °C while the maximum VR conversion (51.4 wt%) was achieved at 450 °C, 2 h, and Wc = 1.5 g. At maximum VR conversion, the weight percent

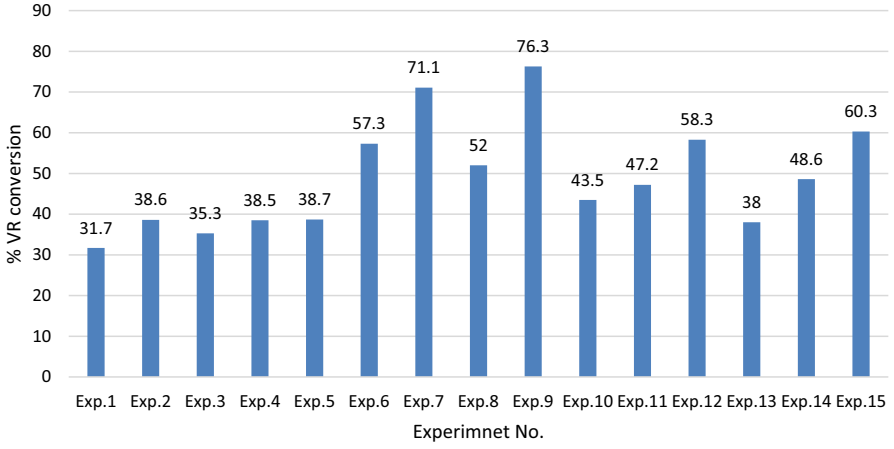

Fig. 4 VR conversation concerning experiments number. Experiments 1 and 2 were at 400–425 °C. Experiments 3, 4, and 5 were at 10 wt steam%, 400 °C reaction temperature, and 2 h reaction time using different ZrFeNi catalyst amounts (0.5, 1, and 1.5 g). Experiments 5, 6, and 7 present the cracking yield at different reaction temperatures (400, 425, and 450 °C) with the same operating conditions (ZrFeNi catalyst, 10 wt steam%, 1.5 g catalyst weight, and 2 h reaction time). Experiments 5, 8, and 9 present the cracking yield of different reaction times (2, 3, and 4 h) with the same operating conditions (ZrFeNi catalyst, 10 wt steam%, 400 °C, and 1.5 g catalyst weight). Experiments 5, 10, and 11 present the cracking yield of different steam loading (10, 15, and 20 wt%) with the same operating conditions (ZrFeNi catalyst, 400 °C, 1.5 g catalyst weight, and 2 h reaction time). Experiment 12 represents the catalytic cracking yield for two feedstock was compared with the same operating conditions (ZrFeNi catalyst, 400 °C, 1.5 g catalyst weight, and 2 h reaction time). Experiments 13, 14, and 15 present the cracking yield at different reaction temperatures (400, 425, and 450 °C) with the same operating conditions (ZrCoNi catalyst, 10 wt steam%, 1.5 g catalyst weight, and 2 h reaction time)

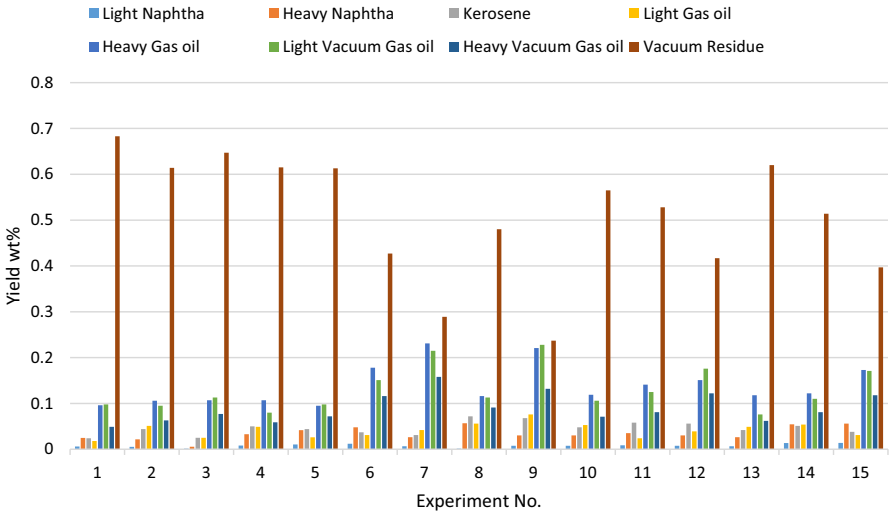

Fig. 5 Desired products yield concerning experiments number. Experiments 1 and 2 were at 400–425 °C. Experiments 3, 4, and 5 were at 10 wt steam%, 400 °C reaction temperature, and 2 h reaction time using different ZrFeNi catalyst amounts (0.5, 1, and 1.5 g). Experiments 5, 6, and 7 present the cracking yield at different reaction temperatures (400, 425, and 450 °C) with the same operating conditions (ZrFeNi catalyst, 10 wt steam%, 1.5 g catalyst weight, and 2 h reaction time). Experiments 5, 8, and 9 present the cracking yield of different reaction times (2, 3, and 4 h) with the same operating conditions (ZrFeNi catalyst, 10 wt steam%, 400 °C, and 1.5 g catalyst weight). Experiments 5, 10, and 11 present the cracking yield of different steam loading (10, 15, and 20 wt%) with the same operating conditions (ZrFeNi catalyst, 400 °C, 1.5 g catalyst weight, and 2 h reaction time). Experiment 12 represents the catalytic cracking yield for two feedstock was compared with the same operating conditions (ZrFeNi catalyst, 400 °C, 1.5 g catalyst weight, and 2 h reaction time). Experiments 13, 14, and 15 present the cracking yield at different reaction temperatures (400, 425, and 450 °C) with the same operating conditions (ZrCoNi catalyst, 10 wt steam%, 1.5 g catalyst weight, and 2 h reaction time)

of cracking products were 0.2% LN, 0.8% HN, 3.6% Ke, 3.6% LGO, 15.5% HGO, 16.4% LVGO, 11.2% HVGO, and 48.6% VR. Also, the VR is mainly converted to HGO, LVGO.

Analysis of kinetic modeling

Kinetic modeling was used to represent the steam catalytic cracking results of the vacuum residue while the new developed kinetic model contained eight lumps that undergo seven different reactions (light naphtha, heavy naphtha, kerosene, light gas oil, heavy gas oil, light vacuum gas oil, heavy vacuum gas oil, and vacuum residue) and 28 reactions. Equations (1–8) were solved using the 4th order Runge–Kutta integration method to determine the model results while the genetic algorithm optimization method was used to estimate optimum kinetic parameters. The predicted kinetic parameters are presented in Table 4. Activation energies did not show a clear pattern and these agree very well with results explored by Félix et al. [33]. All numerical integration and stochastic optimization programs were written using ode45 and

genetic algorithm (GA) commands through MATLAB version 2020a. Seven different experiments (5–11) were used in an acceptable prediction of the reaction kinetic parameters because they covered all the model variables (steam percent, reaction temperature, reaction time, and catalyst weight) as presented in Table 6. Fig. 6 presents a comparison between experimental and predicted weight percent of cracking products and showed that the kinetic model represents the experimental data in a moderately acceptable manner. The mean relative error and mean absolute error were 22.67, and 0.02258, and somewhat moderate because the input data represents a wide range of operating variables.

Conclusions

The main subject of this research was applying a multi-active metal catalyst in cracking of the vacuum residue and studying the effect of cracking operating conditions on the yield of lighter products. X-ray diffraction confirmed a crystalline structure of the synthesized catalyst under 100 °C and therefore it can be considered as completely crystalline with high purity of the framework structure according to its crystallinity degree. SEM images of synthesized catalysts proved the desired catalysts morphology with segregation. VR hydrocracking was performed with/without a presence of manufactured catalysis, but VR conversions of the catalytic cracking are stronger than those of thermal cracking, denoting that both prepared catalysts were active for hydrocracking reactions and the ZrFeNi catalyst was slightly stronger than

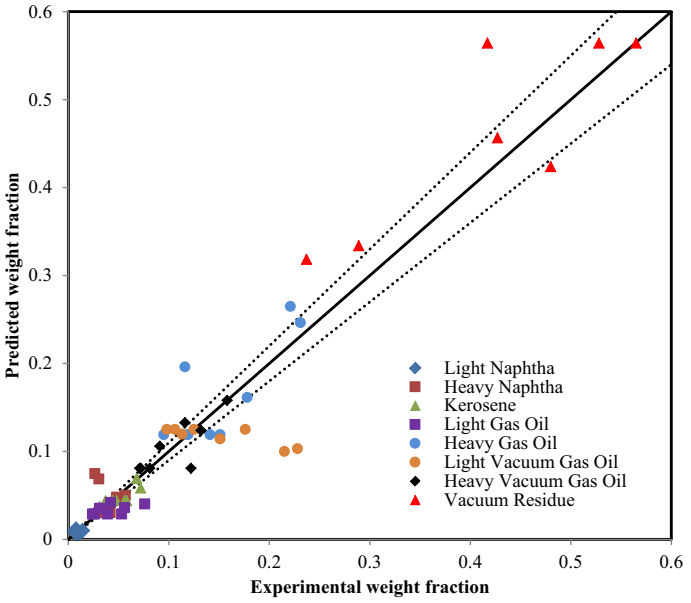

Fig. 6 Comparison between experimental and predicted weight percent of cracking products

the ZrCoNi one. The temperature was the most effective variable for increasing VR conversion, but increasing cracking temperature also increased heavier fractions.

Supplementary Information The online version contains supplementary material available at https://doi.org/10.1007/s11144-022-02179-w.

Acknowledgements The authors would like to thank the Department of Chemical Engineering, University of Technology, Baghdad, Iraq for the support to achieve this study.

Declarations

Conflict of interest The authors have no conflict of interest.

References

1. Hussein ZA, Shakor ZM, Alzuhairi M, Al-Sheikh F (2021) Thermal and catalytic cracking of plastic waste: a review. Int J Environ Anal Chem. https://doi.org/10.1080/03067319.2021.1946527
2. Fumoto E, Sato S, Takanohashi T (2011) Production of light oil by oxidative cracking of oil sand bitumen using iron oxide catalysts in a steam atmosphere. Energy Fuels 25(2):524–527. https://doi.org/10.1021/ef101069m
3. Gai XK, Arano H, Lu P, Mao JW, Yoneyama Y, Lu CX et al (2016) Catalytic bitumen cracking in sub-and supercritical water. Fuel Process Technol 142:315–318. https://doi.org/10.1016/j.fuproc.2015.10.032
4. Ahn HK, Park SH, Sattar S, Woo SI (2016) Vacuum residue upgrading through hydroprocessing with subcritical water. Catal Today 265:118–123
5. Do LT, Nguyen-Huy C, Shin EW (2017) Effect of a Ce y Ni 1− y O 2− δ solid solution on the oxidative cracking of vacuum residue over NiK/CeO 2. React Kinet Mech Catal 122(2):983–993. https://doi.org/10.1007/s11144-017-1252-5
6. Nguyen-Huy C, Shin EW (2017) Oxidative cracking of vacuum residue with steam over NiK/CeZr–Al catalysts. Fuel 192:149–157. https://doi.org/10.1016/j.fuel.2016.12.026
7. Yunanto I, Haryati S, Bustan MD (2019) Pyrolysis of vacuum residue by thermal and catalytic cracking using active alumina catalyst. IJFAC (Indones J Fundam Appl Chem) 4(1):29–34. https://doi.org/10.24845/ijfac.v4.i1.29
8. Puron H, Pinilla JL, Saraev AA, Kaichev VV, Millan M (2020) Hydroprocessing of Maya vacuum residue using a NiMo catalyst supported on Cr-doped alumina. Fuel 263:116717. https://doi.org/10.1016/j.fuel.2019.116717
9. Singh J, Kumar MM, Saxena AK, Kumar S (2005) Reaction pathways and product yields in mild thermal cracking of vacuum residues: a multi-lump kinetic model. Chem Eng J 108(3):239–248. https://doi.org/10.1016/j.cej.2005.02.018
10. Rezaei H, Liu X, Ardakani SJ, Smith KJ, Bricker M (2010) A study of cold lake vacuum residue hydroconversion in batch and semi-batch reactors using unsupported MoS2 catalysts. Catal Today 150(3–4):244–254. https://doi.org/10.1016/j.cattod.2009.10.005
11. Alsobaai AM (2013) Thermal cracking of petroleum residue oil using three level factorial design. J King Saud Univ-Eng Sci 25(1):21–28. https://doi.org/10.1016/j.jksues.2011.06.003
12. AlHumaidan F, Lababidi HM, Al-Rabiah H (2013) Thermal cracking kinetics of Kuwaiti vacuum residues in Eureka process. Fuel 103:923–931. https://doi.org/10.1016/j.fuel.2012.08.005
13. Manek E, Haydary J (2014) Modelling of catalytic hydrocracking and fractionation of refinery vacuum residue. Chem Pap 68(12):1716–1724. https://doi.org/10.2478/s11696-014-0620-0
14. Fumoto E, Sugimoto Y, Sato S, Takanohashi T (2015) Catalytic cracking of heavy oil with iron oxide-based catalysts using hydrogen and oxygen species from steam. J Jpn Petrol Inst 58(5):329–335
15. Lee HS, Nguyen-Huy C, Pham TT, Shin EW (2016) ZrO2-impregnated red mud as a novel catalyst for steam catalytic cracking of vacuum residue. Fuel 165:462–467. https://doi.org/10.1016/j.fuel.2015.10.083

16. Shvets VF, Kozlovskiy RA, Luganskiy AI, Gorbunov AV, Suchkov YP, Ushin NS, Cherepanov AA (2016) Oxygen-induced cracking distillation of oil in the continuous flow tank reactor. Int J Environ Sci Educ 11(11):4855–4868
17. Cabrales-Navarro FA, Pereira-Almao P (2017) Catalytic steam cracking of a deasphalted vacuum residue using a Ni/K ultradispersed catalyst. Energy Fuels 31(3):3121–3131. https://doi.org/10.1021/acs.energyfuels.6b03004
18. Ajumobi OO, Muraza O, Kondoh H, Hasegawa N, Nakasaka Y, Yoshikawa T et al (2018) Upgrading oil sand bitumen under superheated steam over ceria-based nanocomposite catalysts. Appl Energy 218:1–9. https://doi.org/10.1016/j.apenergy.2018.02.161
19. Kaminski T, Husein MM (2019) Kinetic modelling of thermal cracking of Arabian atmospheric and vacuum residue. Fuel Process Technol 189:89–97. https://doi.org/10.1016/j.fuproc.2019.03.007
20. Che Y, Hao J, Zhang J, Qiao Y, Li D, Tian Y (2018) Vacuum residue thermal cracking: product yield determination and characterization using thermogravimetry–fourier transform infrared spectrometry and a fluidized bed reactor. Energy Fuels 32(2):1348–1357. https://doi.org/10.1021/acs.energyfuels.7b03364
21. Wang D, Jin L, Li Y, Wei B, Yao D, Hu H (2019) Upgrading of vacuum residue with chemical looping partial oxidation over Fe-Mn mixed metal oxides. Fuel 239:764–773. https://doi.org/10.1016/j.fuel.2018.11.070
22. Tian Y, Che Y, Chen M, Feng W, Zhang J, Qiao Y (2019) Catalytic upgrading of vacuum residue-derived cracking gas-oil for maximum light olefin production in a combination of a fluidized bed and fixed bed reactor. Energy Fuels 33(8):7297–7304. https://doi.org/10.1021/acs.energyfuels.9b01949
23. Liu B, Zhao K, Chai Y, Li Y, Liu D, Liu Y, Liu C (2019) Slurry phase hydrocracking of vacuum residue in the presence of presulfided oil-soluble MoS2 catalyst. Fuel 246:133–140
24. Shakor ZM (2018) Applying modern optimization techniques for prediction reaction kinetics of Iraqi heavy naphtha hydrodesulferization. Eng Technol J 36(11 Part A):1171–1175
25. Shakor ZM, Ramos MJ, AbdulRazak AA (2020) A detailed reaction kinetic model of light naphtha isomerization on Pt/zeolite catalyst. J King Saud Univ-Eng Sci. https://doi.org/10.1016/j.jksues.2020.12.006
26. Shakor ZM, AbdulRazak AA, Sukkar KA (2020) A detailed reaction kinetic model of heavy naphtha reforming. Arab J Sci Eng 45(9):7361–7370
27. Martínez J, Ancheyta J (2012) Kinetic model for hydrocracking of heavy oil in a CSTR involving short term catalyst deactivation. Fuel 100:193–199. https://doi.org/10.1016/j.fuel.2012.05.032
28. Gao H, Wang G, Xu C, Gao J (2014) Eight-lump kinetic modeling of vacuum residue catalytic cracking in an independent fluid bed reactor. Energy Fuels 28(10):6554–6562. https://doi.org/10.1021/ef501260n
29. Asaee SDS, Vafajoo L, Khorasheh F (2014) A new approach to estimate parameters of a lumped kinetic model for hydroconversion of heavy residue. Fuel 134:343–353. https://doi.org/10.1016/j.fuel.2014.05.079
30. Zheng Y, Tang Q, Wang T, Wang J (2015) Lumping strategy in kinetic modeling of vacuum pyrolysis of plant oil asphalt. Energy Fuels 29(3):1729–1734. https://doi.org/10.1021/ef502530q
31. Taghipour A, Naderifar A (2015) Kinetic modeling of vacuum residue thermal cracking in the visbreaking process using multiobjective optimization. Energy Technol 3(7):758–767. https://doi.org/10.1002/ente.201500029
32. Xu OG, Su HY, Mu SJ, Chu J (2006) 7-Lump kinetic model for residual oil catalytic cracking. J Zhejiang Univ Sci A 7(11):1932–1941. https://doi.org/10.1631/jzus.2006.a1932
33. Félix G, Ancheyta J, Trejo F (2019) Sensitivity analysis of kinetic parameters for heavy oil hydrocracking. Fuel 241:836–844. https://doi.org/10.1016/j.fuel.2018.12.058